Measurements of magnetoresistance in magneto-optical recording media

Cite as: Journal of Applied Physics **69**, 7067 (1991); https://doi.org/10.1063/1.347646
Submitted: 07 September 1990 . Accepted: 11 February 1991 . Published Online: 17 August 1998

Roger A. Hajjar, M. Mansuripur, and H.-P. D. Shieh

Measurements of magnetoresistance in magneto-optical recording media

Roger A. Hajjar and M. Mansuripur
Optical Sciences Center, University of Arizona, Tucson, Arizona 85721

H.-P. D. Shieh
IBM T. J. Watson Research Center, Yorktown Heights, New York 10598

(Received 7 September 1990; accepted for publication 11 February 1991)

The magnetoresistance effect in compositionally modulated transition-metal/transition-metal films (Co/Pt and Co/Pd) and in amorphous binary rare-earth–transition-metal alloy films (TbFe) has been investigated. Results of measurements on several samples at room temperature as a function of the strength of the applied magnetic field are reported. For each sample three different configurations are investigated in which the direction of the applied field is (i) perpendicular to the plane of film, (ii) in the plane of the film and parallel to the direction of the electric current, (iii) in the plane of the film and perpendicular to the direction of the current. During these measurements the extraordinary Hall effect and the magneto-optic Kerr effect have also been monitored. This additional information, together with the magnetization measurement results obtained from a vibrating sample magnetometer, are used to analyze the data and to explain some of their interesting features.

I. INTRODUCTION

Galvanomagnetic phenomena have been known for many years[1–10] and have found practical applications in advanced computer storage technology and semiconductor Hall-effect sensors.[11] They also provide a simple route to measuring some of the electrical, thermal, and magnetic properties of solids. In this paper we focus attention on the changes induced by an applied magnetic field in the electrical resistivity of several thin film samples. These include amorphous binary rare-earth–transition-metal (RE-TM) alloy films of TbFe, as well as compositionally modulated TM/TM films of Co/Pt and Co/Pd. Both classes of material provide suitable recording media for magneto-optical data storage systems, and are currently under worldwide investigation. The magnetoresistance data, obtained at room temperature with the applied magnetic field both parallel and perpendicular to the direction of the electric current, contains valuable information about the magnetic state of the material. The purpose of the present paper is to report the measurement results obtained for a number of samples, and to explain those features of these results that can be understood based on the existing theories. Not every feature of the measured curves is presently understood, and we have tried to be clear about those in the course of our discussions. In addition to the magnetoresistance, we have monitored the Hall voltage and the magneto-optic polar Kerr effect during these measurements. Also measured are the net magnetic moments of the samples using vibrating sample magnetometry. This additional information helps put the magnetoresistance results in perspective and provides a more complete picture of the physical situation.

In Sec. II we outline the design of our experimental setup. Section III contains a brief description of the origins of the various galvanomagnetic effects observed in these experiments. Results of measurements are then presented and discussed in Sec. IV. Closing remarks and conclusions appear in Sec. V.

II. THE EXPERIMENTAL SETUP

In the experiments reported here, the magnetoresistance, Hall effect, and the magneto-optical Kerr effect for each sample were measured simultaneously. The measurements were performed in an electromagnet with maximum field capability of 20 kOe. The magnet has a rotating state that allows its field to be applied both perpendicular to and in the plane of the sample. The three different geometries for measurements of the magnetoresistive and Hall effects are illustrated in Fig. 1. Figure 1(a) shows the perpendicular geometry, where the field is normal to the plane of the sample and the current flows between point contacts 1 and 2. The Hall effect is measured between terminals 3 and 4. In the longitudinal geometry shown in Fig. 1(b) the magnetic field is in the plane of the sample and parallel to the direction of the current, which flows between terminals 1 and 2. The transverse geometry, shown in Fig. 1(c), is similar to the longitudinal case, with the exception that the current terminals are now terminals 3 and 4. The magneto-optical Kerr effect is measured using a normally incident beam from a HeNe laser and a differential detection module that monitors the polarization state of the reflected light.[12]

The alternating current (ac) method is used to measure the magnetoresistance and Hall effects. In addition to eliminating the emf induced by the magnetic-flux variations, the ac technique allows fast and reliable measurements that minimize the voltage drift. Figure 2 illustrates the differential scheme used in processing the electric signals. To minimize the total equivalent rms input noise and eliminate capacitive effects, the drive frequency was set to 5 kHz. The bandwidth of the amplifier is 500 Hz and its gain at the operating frequency is about 200. The resolu-

 0021-8979/91/107067-14$03.00

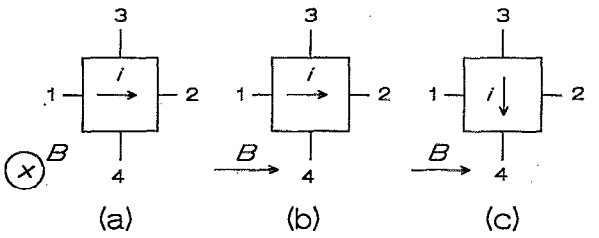

FIG. 1. Three geometries for measurement of the magnetoresistance and the Hall effect.

tion of the resistance measurements is about 100 $\mu\Omega$, while the power dissipation in the sample is kept below 1 mW. The 1×1.5-cm^2 samples were connected to the bridge and to the processing electronics via two mutually orthogonal pairs of point contacts.

III. SOURCES OF MAGNETORESISTANCE AND THE HALL EFFECT

The galvanomagnetic effects may be separated into those which depend on the magnetic induction **B** and those which depend on the magnetization **M**. Let us denote by ρ_0 the ordinary dc resistivity of an otherwise isotropic material in the absence of **B** and **M**, that is, ρ_0 is the resistivity with the exclusion of the magnetic contributions. For a given material under normal conditions, therefore, ρ_0 is a function of temperature only. Contributions of the **B** field to the transport properties are usually classified under the "ordinary" effects, whereas those stemming from the magnetization are referred to as "anomalous" or "extraordinary."

The most common galvanomagnetic effects are the ordinary magnetoresistance (MR) and the ordinary Hall effect.[4,10] These effects are caused by the Lorentz force acting on conduction electrons. A naive description of the ordinary magnetoresistance, for example, maintains that the B field gives the conduction electrons a curved path, thereby increasing their frequency of collisions with phonons/impurities, and resulting in an increased electrical resistance.[10] Ordinary MR is best observed in nonmagnetic metals and semiconductors; the effect is appreciable if the mean free path of the conduction electron is large compared with its radius of curvature in the magnetic field. In amorphous materials and in polycrystalline specimens composed of very small crystallites, the mean free path is short and the ordinary MR is consequently small. Ordinary MR in thin films is further reduced due to the surface scattering of the conduction electrons, which tends to shorten the mean free path. In ferromagnetic metals, the exchange interaction between conduction electrons and the magnetic ions reduces the mean free path, resulting in lower ordinary MR at elevated temperatures. Ordinary MR, however, may assert itself at low temperatures due to the increased order of the magnetic lattice.

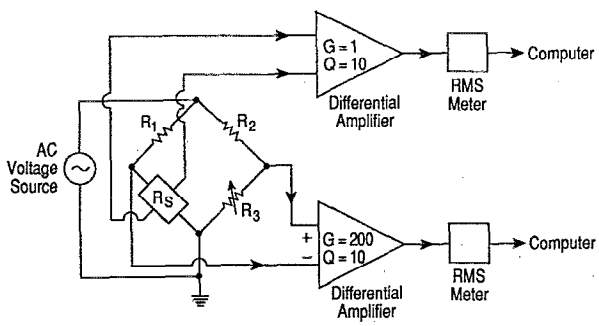

FIG. 2. The differential scheme used for processing the electrical signals.

At fields not too large and temperatures not too small, ordinary MR is usually a parabolic function of the applied field, its magnitude increasing with the square of the effective B field. There are exceptions to this rule, however. For example, under proper circumstances when the field and the current are both in the plane of a thin film and parallel to each other, the spiraling electrons could avoid the film surface and result in a decreasing resistivity with an increasing field. Ordinary magnetoresistance is longitudinal when the **B** field is parallel to the direction of the electric current and transverse when the two are orthogonal. In ordinary MR the transverse effect is generally observed to be larger than the longitudinal effect.

The following resistivity tensor describes both the magnetoresistance and the Hall effect in compact form:

$$\Delta\rho=\begin{pmatrix}\rho_{xx} & \rho_{xy} & 0\\ -\rho_{xy} & \rho_{xx} & 0\\ 0 & 0 & \rho_{zz}\end{pmatrix}. \tag{1}$$

$\Delta\rho$ in Eq. (1) is the incremental resistivity, contributed by a **B** field along the z axis, to the isotropic base resistivity ρ_0 of the material. In this formula ρ_{xx} is the transverse magnetoresistivity, ρ_{zz} is the longitudinal magnetoresistivity, and ρ_{xy} is the Hall resistivity. These elements of the resistivity tensor depend on B, of course. At $B=0$ they are all equal to zero; in low and moderate fields, ρ_{xx} and ρ_{zz} are usually quadratic functions of B whereas ρ_{xy} is linear in B. For arbitrary orientations of B, the MR tensor in Eq. (1) must be transformed with the aid of appropriate rotation matrices. For instance, if **B** happens to be in the yz plane at an angle Θ relative to the z axis, the rotation matrix will be

$$R=\begin{pmatrix}1 & 0 & 0\\ 0 & \cos\Theta & -\sin\Theta\\ 0 & \sin\Theta & \cos\Theta\end{pmatrix}. \tag{2}$$

Consequently, the resistivity tensor becomes

$$\Delta\rho' = R^T(\Delta\rho)R = \begin{pmatrix} \rho_{xx} & \rho_{xy}\cos\Theta & -\rho_{xy}\sin\Theta \\ -\rho_{xy}\cos\Theta & \rho_{xx}+(\rho_{zz}-\rho_{xx})\sin^2\Theta & \tfrac{1}{2}(\rho_{zz}-\rho_{xx})\sin 2\Theta \\ \rho_{xy}\sin\Theta & \tfrac{1}{2}(\rho_{zz}-\rho_{xx})\sin 2\Theta & \rho_{xx}+(\rho_{zz}-\rho_{xx})\cos^2\Theta \end{pmatrix}. \tag{3}$$

As an example, consider the electric current density j along the y axis, that is, $j=(0,1,0)\,j$. The electric field vector E produced by this current and the resistivity tensor in Eq. (3) is given by

$$\begin{pmatrix} E_x \\ E_y \\ E_z \end{pmatrix} = \Delta\rho' \begin{pmatrix} 0 \\ 1 \\ 0 \end{pmatrix} j = \begin{pmatrix} \rho_{xy}\cos\Theta \\ \rho_{xx}+(\rho_{zz}-\rho_{xx})\sin^2\Theta \\ \tfrac{1}{2}(\rho_{zz}-\rho_{xx})\sin 2\Theta \end{pmatrix} j. \tag{4}$$

Accordingly, the Hall resistivity along x is $\rho_{xy}\cos\Theta$, while the resistivity along y is $\rho_0+\rho_{xx}+(\rho_{zz}-\rho_{xx})\sin^2\Theta$.

Another galvanomagnetic phenomenon, usually observed in transition metals and their alloys, is the reduction of resistivity with increasing magnetic field. This effect was explained by Mott[2] as related to the scattering of the conduction s electrons into the d band. The effect has been mainly studied in ferromagnetic materials, but if the structure of the d band permits, it can appear in nonferromagnetic metals as well.[4] Mott assumes that electrical conduction in transition metals is mainly due to the s electrons, since the d electrons are more strongly bound with the ions and, consequently, have a large effective mass. He also assumes that the scattering of the conduction electrons is a spin-preserving process. Now, in a ferromagnetic transition metal (or alloy) the d band is exchange split between the spin-up ($d\uparrow$) and spin-down ($d\downarrow$) electrons. Let the Fermi level be close to the upper edge of the $d\uparrow$ band. At low temperatures this band ($d\uparrow$) is almost full and has no vacancies for additional spin-up electrons. Thus, if an s electron with spin up is to be scattered during a collision, it can only go to another (available) level in the s band as dictated by the Pauli exclusion principle. At elevated temperatures, however, some of the electrons near the Fermi surface in $d\uparrow$ move to the $d\downarrow$ band. This creates vacancies in $d\uparrow$, thus raising the probability of scattering from the conduction band into the $d\uparrow$ band, and resulting in a higher resistivity.

If we now allow the temperature to be fixed at a reasonably high value and apply a field in the magnetization direction, we shall observe the following phenomenon: As the field increases some of the electrons move back from $d\downarrow$ to $d\uparrow$ and the resistivity subsequently declines. (Obviously, the material need not be ferromagnetic for this mechanism to work. It can happen in a nonferromagnetic metal or in a ferromagnet above the Curie temperature as well, provided that the Fermi level is sufficiently close to the upper edge of the d band.) For a given electron with spin magnetic moment μ_B, the difference in energy between spin-up and spin-down states in a magnetic field $\mathbf{B}$ is $2B\mu_B$. At $B\simeq 20$ kG this energy difference is only 4×10^{-16} erg, which is two orders of magnitude less than k_BT at room temperature. Thus at ordinary temperatures and fields we expect the reduction in resistivity to be small (though by no means inconsequential). Note also that according to this argument the filling of the $d\uparrow$ band (at $B\simeq 20$ kG) will not result in a substantial increase in the saturation magnetization of the material.

Kasuya[3] observed that the negative magnetoresistance also occurs in rare-earth metals, although transitions between s and f bands in these media are unlikely. He argued that the f electron moments, while localized at their lattice sites, interact with the conduction electrons via exchange and spin-orbit mechanisms. At absolute zero of temperature, all the magnetic dipole moments of the f electrons are ordered on the periodic lattice of the crystal, and the magnetic scattering must therefore vanish. At temperatures above zero, this order is disturbed and the conduction electron scattering from the magnetic moments leads to an increase in resistivity. Under these circumstances, the application of a magnetic field tips the balance in favor of magnetic alignment, causing the resistivity once again to decline.

The third galvanomagnetic phenomenon that is specific to magnetically ordered media is the magnetoresistance/Hall effect induced by scattering from the magnetic moments. This effect, whose magnitude also depends on the relative orientation of the magnetization and the current, has been analyzed by Smit[6] and by Kondo[7] who attributed it to the interaction between the spin system and the lattice via the spin-orbit coupling. These authors showed that the conduction electrons moving parallel (or antiparallel) with the direction of magnetization are more easily scattered than those traveling in a transverse direction. When the spin of the magnetic electron is aligned with the direction of the current, its orbital moment is likewise aligned due to the spin-orbit coupling. Since the plane of the orbit is perpendicular to the angular momentum, in this position the magnetic electron exhibits the largest cross section towards the conduction electrons, thus creating the largest resistivity.

The extraordinary galvanomagnetic effects may be analyzed phenomenologically, using a resistivity tensor similar to the one described earlier in conjunction with the ordinary effects. The extraordinary tensor has the same form as in Eq. (1), but the z axis should be designated as the direction of the magnetization of the single-domain specimen. ρ_{xy} is now the coefficient of the extraordinary Hall effect. In contrast to the case of ordinary MR, the longitudinal extraordinary resistivity ρ_{zz} is generally larger than the corresponding transverse resistivity ρ_{xx}.

IV. EXPERIMENTAL RESULTS AND DISCUSSION

A large number of samples were characterized in our experiments. Eight of these samples were chosen as representative and the corresponding results will be described in the following subsections. The measured data for the first sample (a Co/Pt superlattice) is discussed in detail, complete with explanation of those features that are presently understood. Other samples are given a shorter treatment, simply because many of their characteristics are similar to the first sample; only those features that are different are emphasized. The second sample is a Co/Pd superlattice. The third sample, a thin film of polycrystalline cobalt, is not an optical recording medium but is included here for comparison with the superlattice films.

The remaining five samples are amorphous films of Tb_xFe_{1-x} with different values of x, but similar as far as fabrication conditions are concerned. The atomic percentages of terbium in these samples are $x = 28$, 24, 22.5, 20.3, and 18.3. The compensation point temperature for the first three of these samples is greater than 300 K, making them terbium rich, that is, at room temperature their net magnetization is dominated by Tb. the last two samples have a compensation point below the room temperature and are therefore iron rich. Recently, magnetoresistance measurement of TbFeCo films has been reported by Yumoto *et al.*[9] Although we find agreement between their data and ours in some cases, there are disagreements in others; our interpretation of some of the results is also different from theirs. The measurements of Yumoto *et al.* were confined to the perpendicular field geometry, whereas our data includes the longitudinal and transverse geometries as well.

Samples and measurement data for inclusion in this section have been selected carefully in order to avoid redundancy while presenting all the available information that is deemed useful. Certain features of the data can be explained from the existing theories of magnetoresistance and thin-film micromagnetics. There are, however, other interesting features which are not readily understood. We have thus included a comprehensive collection of data for each sample that not only brings the unusual characteristics to the fore, but also provides sufficient information for those who might be inclined to try new or alternative explanations.

A. Co/Pt superlattice

The sample was an e-beam-evaporated Co/Pt superlattice on glass substrate, composed of twenty periods of alternating layers of Co (5 Å) and Pt (10 Å), with a total thickness of 300 Å. Results of vibrating sample magnetometry (VSM) measurements on this sample at room temperature are shown in Fig. 3(a). The easy axis is perpendicular and the sample has saturation moment $M_s = 410$ emu/cm^3 and coercive field $H_c = 1.3$ kOe. The reversal process takes place by a rapid nucleation of domains at $H = H_c$, resulting in the steep part of the hysteresis loop, followed by a rather slow growth of these domains that requires an additional field of ~ 1 kOe for the completion of the reversal process.

The VSM curve obtained with an applied in-plane field [dashed curve in Fig. 3(a)] shows a steep rise in the vicinity of $H = 0$. Since the sample is in a demagnetized state, this steep rise is probably due to domain-wall motion and/or alignment of the in-plane components of magnetization. At larger field values the slope of the curve is due to rotation of magnetization away from the (perpendicular) easy axis and towards the direction of the applied field. Extrapolating from the slope of this curve at intermediate values of the applied field, one obtains the anisotropy field of $H_k = 2K_u/M_s - 4\pi M_s \simeq 12$ kOe. The uniaxial anisotropy energy constant for the sample is thus obtained as $K_u \simeq 3.56 \times 10^6$ erg/cm^3.

Starting from a demagnetized state and applying the magnetic field perpendicular to the plane of the sample, we obtained the Hall loop shown in Fig. 3(b). The Hall resistivity in the saturated state is $\rho_{xy} = 1.2$ $\mu\Omega$ cm. The coercive field value and other features of this loop are similar to the VSM loop. The result of measurement of the Hall effect when the sample is initially saturated in the perpendicular direction and the applied field is in plane is shown in Fig. 3(c). The initial slow decrease in the Hall voltage (which is reversible) is due to the rotation of **M** towards the field. Following this initial phase, the rapid (irreversible) drop in the Hall voltage indicates the breakup of the magnetization into oppositely magnetized domains. (This breakup into domains is not predicted by the coherent rotation theory of Stoner and Wohlfarth,[13] but occurs in practice probably due to the existence of inhomogeneities in the sample such as regions with slightly different axes of anisotropy. An alternative explanation for the breakup into domains involves the changing balance between domain-wall energy and demagnetizing energy.) Finally, at sufficiently large fields, the magnetization comes into alignment with the field, at which point the Hall voltage becomes negligibly small. Reducing the magnetic field now back to zero does not yield the original Hall voltage, simply because the sample is no longer saturated. The small hysteresis loop in Fig. 3(c), obtained by sweeping the field, is repeatable and is probably due to the motion of domain walls in the demagnetized state. Alternatively, this hysteretic behavior might be related to the small deviations of the local easy axis across the sample.

The polar magneto-optical Kerr effect was also measured for this sample. The hysteresis loop (obtained in a perpendicular field) is shown in Fig. 3(d). The maximum Kerr angle is $\Theta_k = 0.25°$ and the loop is identical with the Hall loop. When the saturated film (along the easy axis) was subjected to an in-plane field, the polar Kerr signal behaved as in Fig. 3(e), once again in agreement with the corresponding Hall effect measurement. The value of H_k estimated from the curvature of the initial part of this curve (near the top) is about 11 kOe, in fairly good agreement with the VSM estimate. The similarity between the Kerr-effect and the Hall-effect signals is remarkable, considering the fact that the laser beam illuminates only a small fraction of the total sample area.

Figure 3(f) is a plot of $\Delta\rho/\rho$ vs H, where H is the magnitude of the applied field perpendicular to the plane of

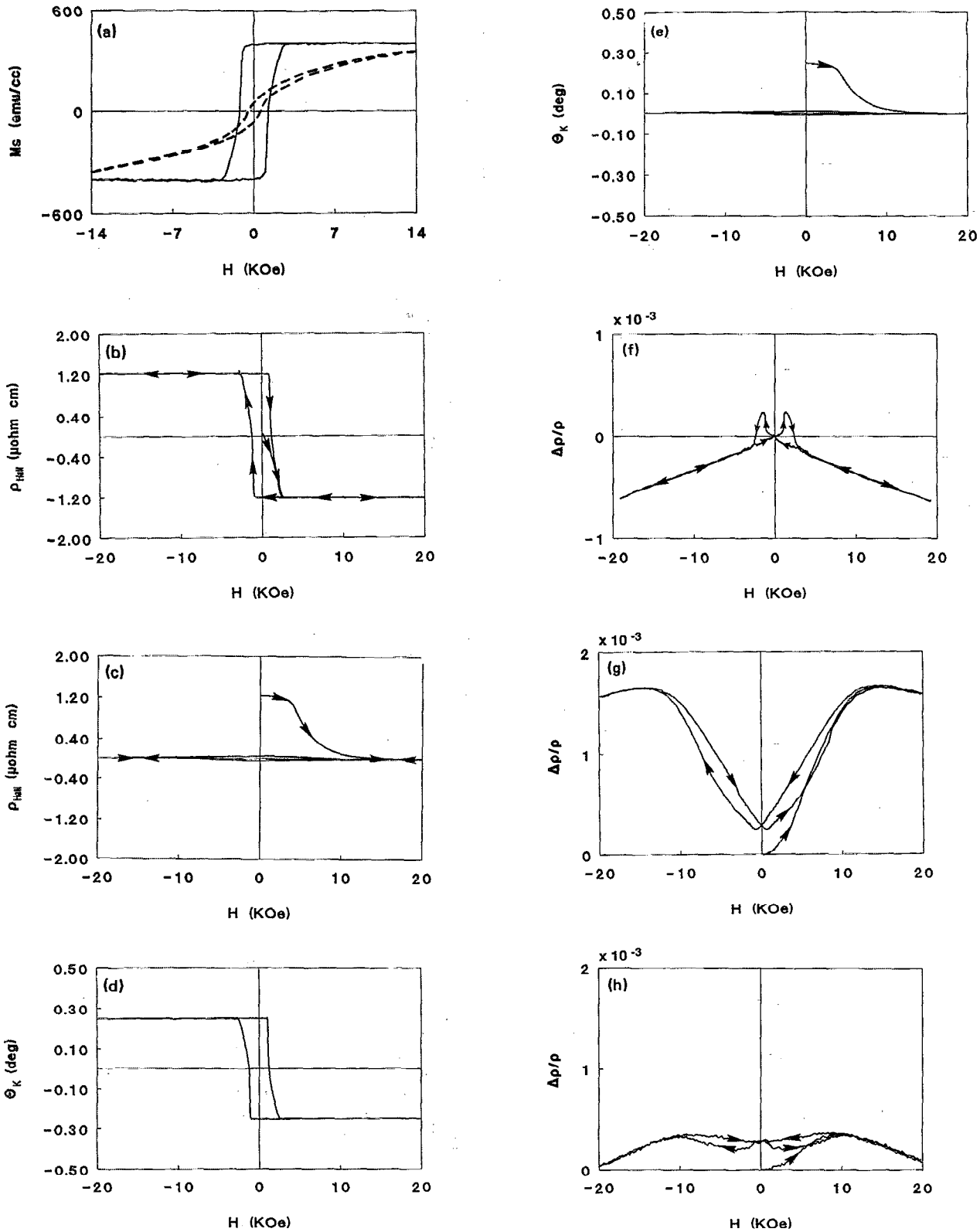

FIG. 3. Results of various measurements on a Co/Pt sample (5-Å-thick cobalt layers alternating with 10-Å-thick platinum layers, with a total thickness of 300 Å). (a) VSM measurement with the magnetic field perpendicular (solid curve) and in the plane of the sample (dashed curve). (b) Hall resistivity vs the magnitude of an applied perpendicular field. The initial state of the sample is demagnetized. (c) Hall resistivity vs the magnitude of an applied in-plane field. The sample is initially in the saturated state. (d) Magneto-optic polar Kerr signal vs the magnitude of an applied perpendicular field. The sample is initially saturated. (e) Magneto-optic polar Kerr signal vs the magnitude of an applied in-plane field. The initial state of the sample is saturated. (f) Resistivity variation as function of the magnitude of an applied perpendicular field. (g) Resistivity variation with applied field in the longitudinal geometry. The sample is initially saturated along the easy axis (i.e., in the perpendicular direction). (h) Resistivity variation with applied field in the transverse geometry.

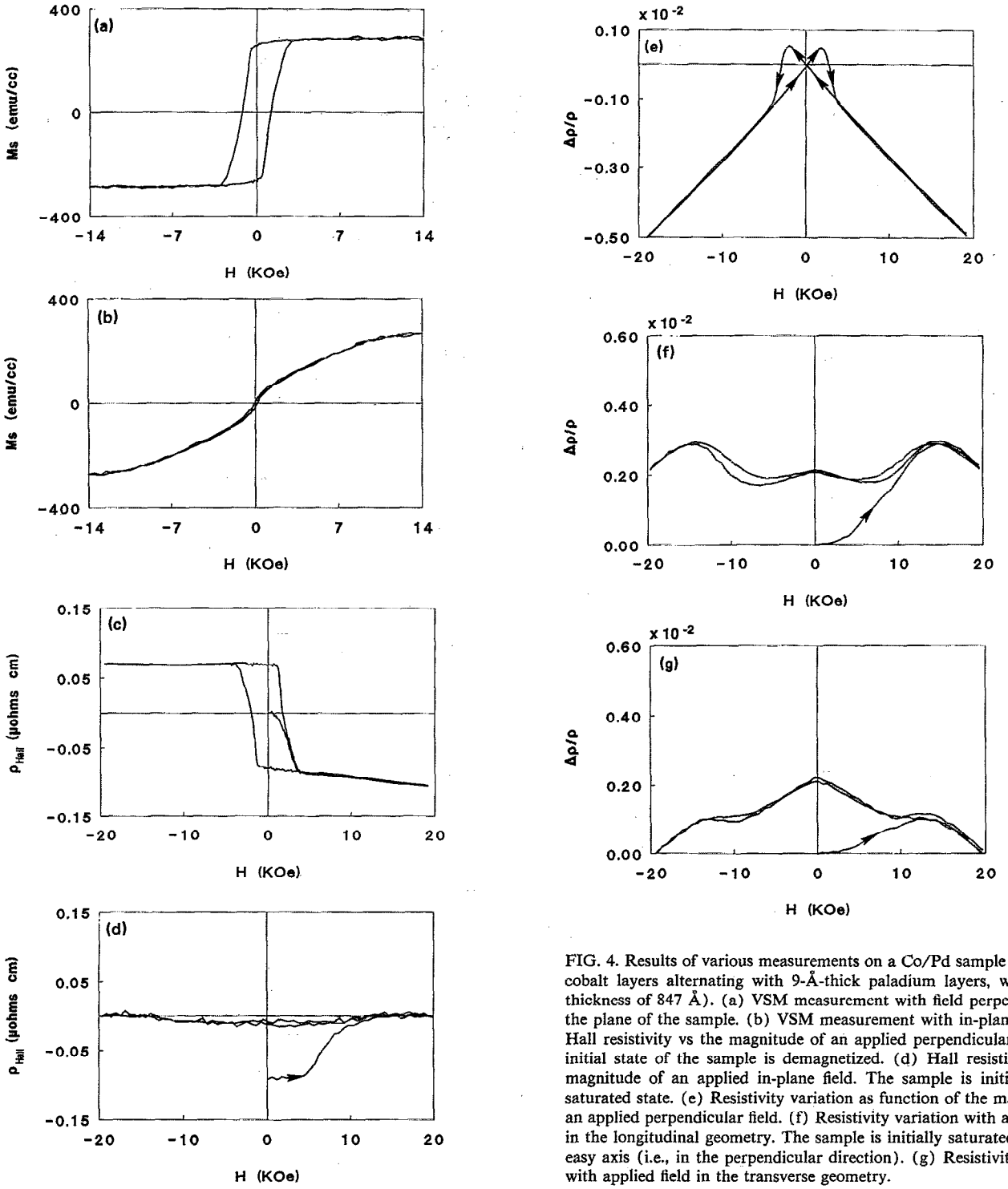

FIG. 4. Results of various measurements on a Co/Pd sample (2-Å-thick cobalt layers alternating with 9-Å-thick paladium layers, with a total thickness of 847 Å). (a) VSM measurement with field perpendicular to the plane of the sample. (b) VSM measurement with in-plane field. (c) Hall resistivity vs the magnitude of an applied perpendicular field. The initial state of the sample is demagnetized. (d) Hall resistivity vs the magnitude of an applied in-plane field. The sample is initially in the saturated state. (e) Resistivity variation as function of the magnitude of an applied perpendicular field. (f) Resistivity variation with applied field in the longitudinal geometry. The sample is initially saturated along the easy axis (i.e., in the perpendicular direction). (g) Resistivity variation with applied field in the transverse geometry.

the film and ρ is the initial resistivity at $H=0$. (Using the van der Pauw method,[14] the value of ρ in the remanent state was found to be 58 $\mu\Omega$ cm.) The linear part of the curve, with a negative slope of 3.2×10^{-8} per Oe, has its origin in the *s-d* scattering phenomenon described in Sec. III. The peaks centered around the coercive field are caused by the scattering of the conduction electrons from the magnetization within the domain walls. These walls (which are inevitably present during the formation and growth of reverse-magnetized domains) cause the resistivity to increase provided that their magnetic moments, while in the plane of the film, are also parallel to the direction of the current. Thus the height of the peaks in Fig. 3(f) is a measure of the volume fraction covered by the domain walls, while the width of the peaks corresponds to the transition region observed in the vicinity of H_c in the hysteresis loop.

Figure 3(g) shows the measured values of $\Delta\rho/\rho$ vs H,

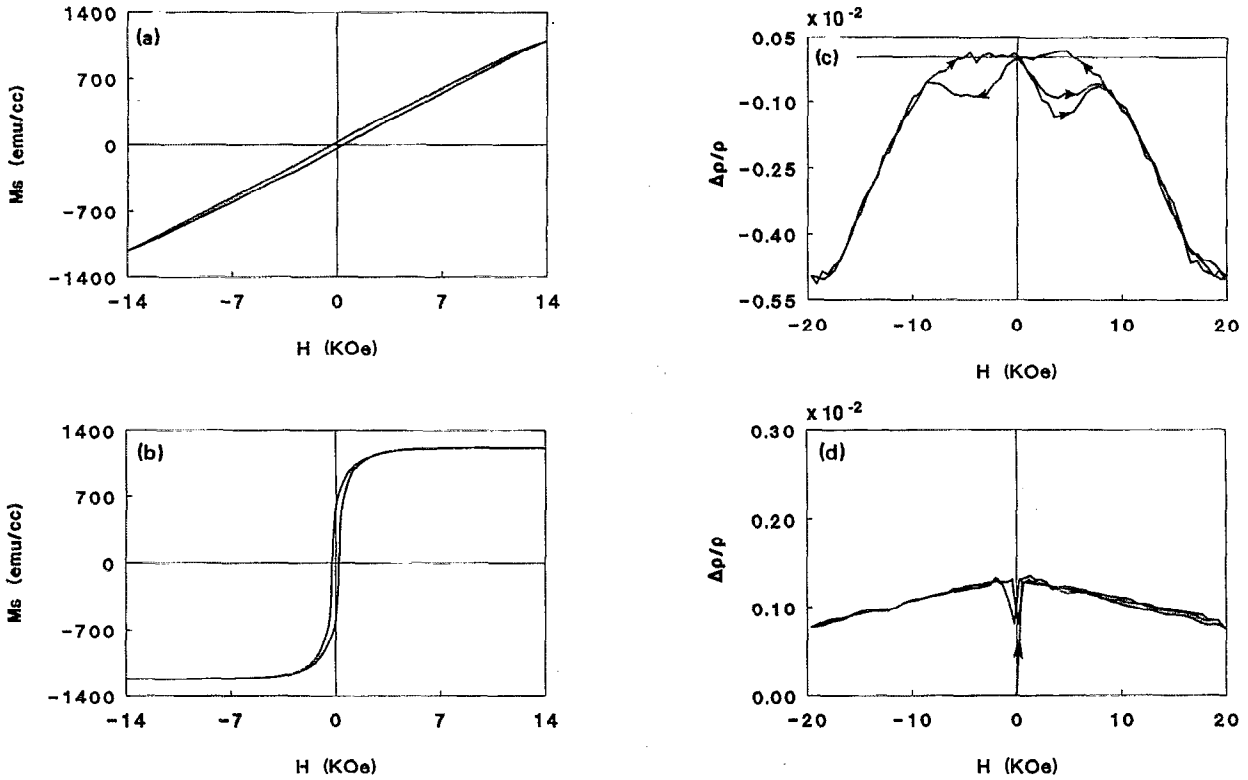

FIG. 5. Results of various measurements on a pure cobalt sample with a thickness of 1750 Å: (a) VSM measurement with field perpendicular to the plane of the sample; (b) VSM measurement with in-plane field; (c) resistivity variation as function of the magnitude of an applied perpendicular field; (d) resistivity variation with applied field in the longitudinal geometry.

where H is the magnitude of the longitudinal field applied in the plane of the sample and parallel to the direction of the current. At first, the sample is saturated along the easy axis. The initial increase of the resistance with H is due mainly to the alignment of the magnetization vector $\mathbf{M}$ with the current. As expected, the maximum is reached around $H = H_k \simeq 12$ kOe. Once the magnetization and the field have been aligned, further increases in H cause a linear decrease of $\Delta\rho/\rho$ which, as before, is due to *s-d* scattering. It is important to realize that the *s-d* mechanism can become effective only after full alignment between the magnetization and the field has been achieved. (The justification for this statement will be given later in the section.) Thus, ignoring the ordinary MR effects, one can associate the maximum rise of 1.65×10^{-3} in $\Delta\rho/\rho$ with $(\rho_{zz} - \rho_{xx})/\rho$ corresponding to the extraordinary effect.

Let us denote by Θ the angular deviation of magnetization from the easy axis. Assuming that the uniaxial anisotropy energy density is given by

$$U = K_u \sin^2\Theta, \tag{5}$$

the Stoner–Wohlfarth model[13] predicts a linear dependence of $\sin\Theta$ on the magnitude of the applied in-plane field, that is,

$$\sin\Theta = H/H_k. \tag{6}$$

Thus, in accordance with the analysis of the previous section,

$$\Delta\rho = (\rho_{zz} - \rho_{xx})(H/H_k)^2, \quad 0 \leqslant H \leqslant H_k. \tag{7}$$

The shape of this function, however, does not quite agree with the experimental data: The relevant part of the curve in Fig. 3(g) lies somewhat above the quadratic function of Eq. (7). We speculate that the disagreement between the coherent rotation theory and experiment in this instance is caused by the breakdown of magnetization into domains, which occurs at $H \simeq 4$ kOe.

Earlier in the section we asserted that the *s-d* mechanism becomes effective only after the magnetization vector $\mathbf{M}$ has aligned itself with the applied in-plane field. The explanation lies in the fact that the effective field acting on $\mathbf{M}$ is given by

$$\mathbf{H}_{\text{eff}} = (H_k \cos\Theta)\,\hat{z} + H\hat{x}, \tag{8}$$

where the first term is the effective anisotropy field acting along the easy axis z, and the second term is the applied field (assumed to be along x). Replacing H in Eq. (8) with $H_k \sin\Theta$ from Eq. (6) yields a net effective field of magnitude H_k along the direction of magnetization. Thus the total effective magnetic field acting on $\mathbf{M}$ during its transition from the easy axis to the plane is a constant, independent of Θ. Consequently, the *s-d* scattering probabilities are unaffected by the magnitude of the applied field H until the magnetization reaches the plane. This occurs at $H = H_k$ which, as corroborated by the data in Fig. 3(g), is the onset of contribution of the *s-d* effect to magnetoresistance.

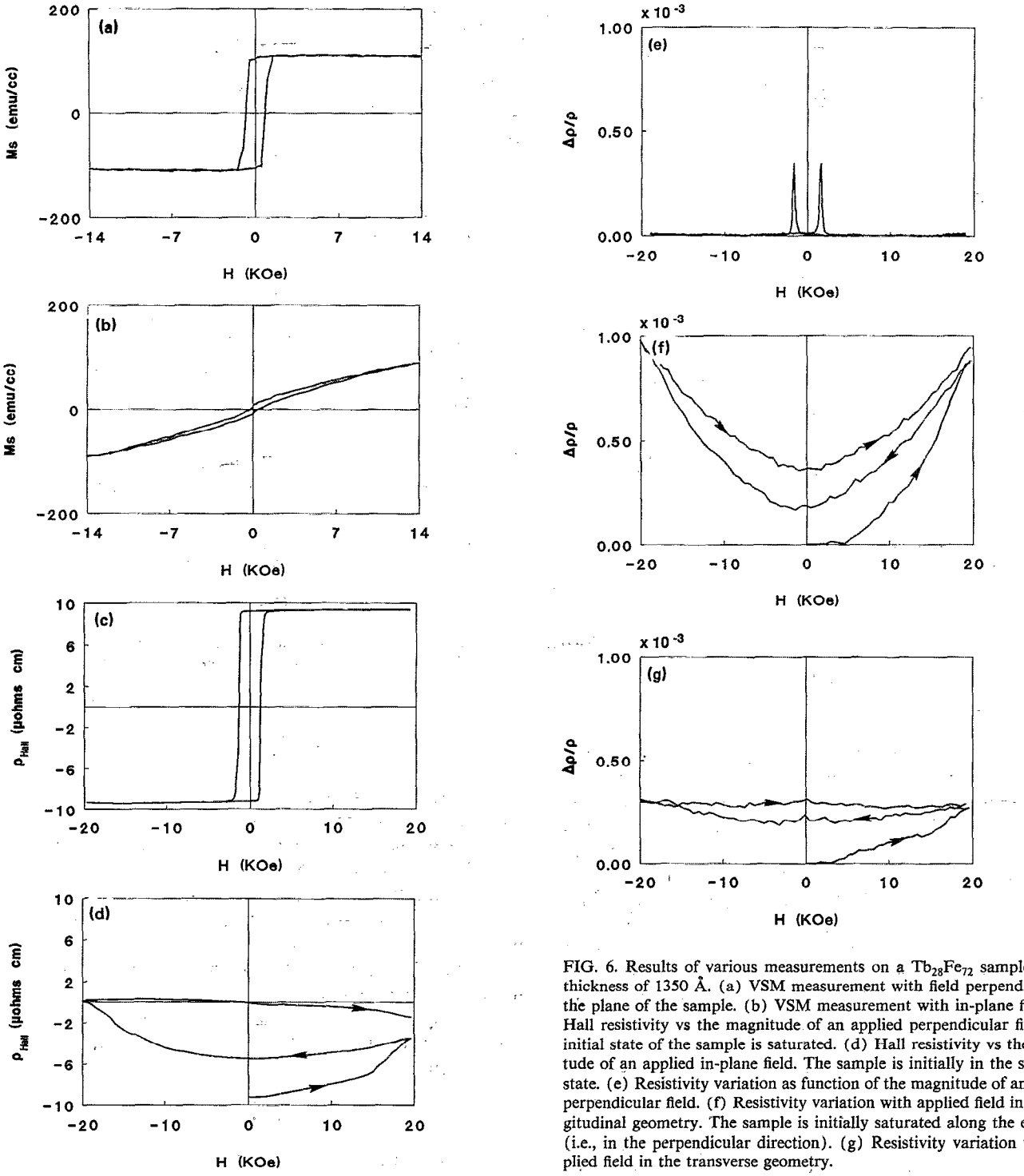

FIG. 6. Results of various measurements on a $Tb_{28}Fe_{72}$ sample with a thickness of 1350 Å. (a) VSM measurement with field perpendicular to the plane of the sample. (b) VSM measurement with in-plane field. (c) Hall resistivity vs the magnitude of an applied perpendicular field. The initial state of the sample is saturated. (d) Hall resistivity vs the magnitude of an applied in-plane field. The sample is initially in the saturated state. (e) Resistivity variation as function of the magnitude of an applied perpendicular field. (f) Resistivity variation with applied field in the longitudinal geometry. The sample is initially saturated along the easy axis (i.e., in the perpendicular direction). (g) Resistivity variation with applied field in the transverse geometry.

It is seen in Fig. 3(g) that when H is brought back to zero the resistance is somewhat larger than its initial value. This is to be expected, simply because the sample is no longer saturated. The difference in $\Delta\rho/\rho$ between the initial (saturated) state and the demagnetized state is about 3.0×10^{-4}, which is somewhat larger than the height of the peaks in Fig. 3(f). Thus the two demagnetized states, one created by a perpendicular field and the other by an *in-plane* field, have slightly different structures.

In Fig. 3(h) we show the measured values of $\Delta\rho/\rho$ vs H, where H is the magnitude of the transverse field applied in the plane of the sample and perpendicular to the direction of the current. Starting from the state of magnetization saturated long the easy axis, the resistance is seen to increase at first, peaking at $H\simeq10$ kOe before it begins to decrease. As in the previous case, the linear decrease with a slope of 3.1×10^{-8} per Oe at $H > H_k$ is due to the *s-d* scattering effect. The initial increase and then decrease of

$\Delta\rho/\rho$ is partly due to the breakup of the saturated state into various domains. There is also the possibility that the geometry of the probes inadvertently permits a fraction of the current to flow along the direction of the field, thus enabling the current to sense the magnetization **M** as it moves into the plane. In any event, certain features of this curve are puzzling and we do not claim to understand it fully.

B. Co/Pd superlattice

The Co/Pd superlattice sample was composed of 77 periods of alternating layers of Co (2Å) and Pd (9 Å), with a total thickness of 847 Å. The film was sputtered on a glass substrate and had perpendicular easy axis. Results of various measurements on this sample are presented in Fig. 4. This sample's characteristics are similar to the Co/Pt sample discussed above; therefore, we proceed to explain only the significant differences between the two.

The saturation magnetization is $M_s \simeq 300$ emu/cm^3 and the anisotropy field as extracted from the VSM data is $H_k \simeq 11$ kOe, yielding the value of $K_u \approx 2.2\times 10^6$ erg/cm^3. In the state saturated along the easy axis, this sample has zero-field resistivity of $\rho = 77$ $\mu\Omega$ cm and Hall resistivity of $\rho_{xy} = 0.075$ $\mu\Omega$ cm. The Hall resistivity as a function of the applied in-plane field in Fig. 4(d) shows the onset of demagnetization at $H \simeq 4$ kOe. The value of the anisotropy field derived from the initial part of the curve in Fig. 4(d) is $H_k \simeq 10$ kOe, which is fairly close to the VSM estimate. The Kerr-effect measurements gave results that were identical to the Hall-effect data and are therefore omitted. The Kerr rotation angle Θ_k for this sample was found to be only 0.05°.

The peak of the longitudinal MR curve in Fig. 4(f) yields the value of 3×10^{-3} for $(\rho_{zz} - \rho_{xx})/\rho$. All the MR curves show the *s-d* effect with a negative slope of 25×10^{-8} per Oe, which is substantially greater than the corresponding slope observed for the Co/Pt sample. This difference is probably related to the position of the Fermi energy E_f in Pd and Pt relative to the edge of the *d* band. According to Mott,[2] the temperature dependence of the resistivity of these metals indicates that in paladium E_f is closer to the edge of the *d* band than in platinum, thus providing one possible explanation for the larger *s-d* effect in our Co/Pd samples. Other possible causes, such as magnetic polarization of the paladium layers at their interfaces with cobalt, however, cannot be discarded.

C. Polycrystalline thin film of pure cobalt

The 1750-Å-thick cobalt film used in these measurements was sputter-deposited on a glass substrate. Shape anisotropy is dominant for this sample and the magnetization lies in the plane of the film. The results presented here are helpful in relating the behavior of the two superlattice samples studied above to the properties of their main magnetic constituent, cobalt. Figure 5(a), obtained from a VSM measurement with perpendicular magnetic field, indicates the linear increase of magnetization along the direction of the applied field. In the absence of other sources of anisotropy, the critical field at which the magnetization becomes fully oriented in the perpendicular direction is $H = 4\pi M_s$. (Saturation magnetization of pure cobalt is $M_s = 1422$ emu/cm^3, thus the alignment should occur at $H \simeq 17.8$ kOe. The maximum available field of the VSM, however, is only 14 kOe, preventing a direct verification of the preceding statement.) Figure 5(b), which shows the results of VSM measurement with an in-plane applied field, clearly indicates the rapid approach to saturation as well as the small value of the in-plane coercivity. Figure 5(c) is a plot of the magnetoresistance $\Delta\rho/\rho$ versus the strength of the applied perpendicular field. (The resistivity of this sample at $H = 0$ was $\rho \simeq 12$ $\mu\Omega$ cm.) Initially, the resistivity decreases due to the alignment of **M** with **H**, which results in a reduced projection of **M** along the direction of the current. At $H \simeq 17$ kOe, however, the magnetization is in complete alignment with **H**, at which point further reductions in resistivity should be attributed to the *s-d* scattering effect. Finally, Fig. 5(d) shows the variation of resistivity with an applied in-plane field (longitudinal geometry). The rapid initial rise in $\Delta\rho/\rho$ is due to the alignment of magnetization with the field. The negative slope of 3.3×10^{-8} per Oe that is observed beyond this initial phase is, once again, a manifestation of the *s-d* scattering phenomenon. Notice that the magnitude of the *s-d* effect for cobalt is very close to that for the Co/Pt superlattices, but much smaller than the slope obtained for the Co/Pd samples.

D. Amorphous $Tb_{28}Fe_{72}$ film

The measurement results for this 1350-Å-thick sample, which was sputter-deposited on glass and had a perpendicular easy axis, are shown in Fig. 6. The net magnetization of the film is $M_s = 115$ emu/cm^3 and its anisotropy field as extracted from the VSM data is $H_k \simeq 16$ kOe. When saturated along the easy axis, the sample exhibited a zero-field resistivity $\rho = 580$ $\mu\Omega$ cm, Hall resistivity $\rho_{xy} = 9.2$ $\mu\Omega$ cm, and Kerr rotation angle $\Theta_k = 0.32°$. The curvature of the Hall voltage versus the applied in-plane field in Fig. 6(d) yields $H_k \simeq 20$ kOe, which is somewhat larger than the VSM estimate. Not shown in Fig. 6 are the field dependencies of the Kerr signal which were the same as those for the Hall signal.

The main difference between this sample and the previously considered superlattice samples is the lack of the negative slope (attributed to *s-d* scattering) in the MR signals. The *s-d* effect due to iron, if anything, should be positive for the present sample, simply because this is a Tb-rich alloy and the iron moment is always in the opposite direction to the saturation moment. The lack of any measurable *s-d* effect is probably due to the particular band structure of iron, which is known to be significantly different from that of cobalt. (The Fermi level in iron is well below the edge of the *d* band.) Also, there is always the possibility that the *s-d* effect is masked by something else, such as the alignment of terbium moments with the applied field which, according to Kasuya's model, could result in reduced resistivity.

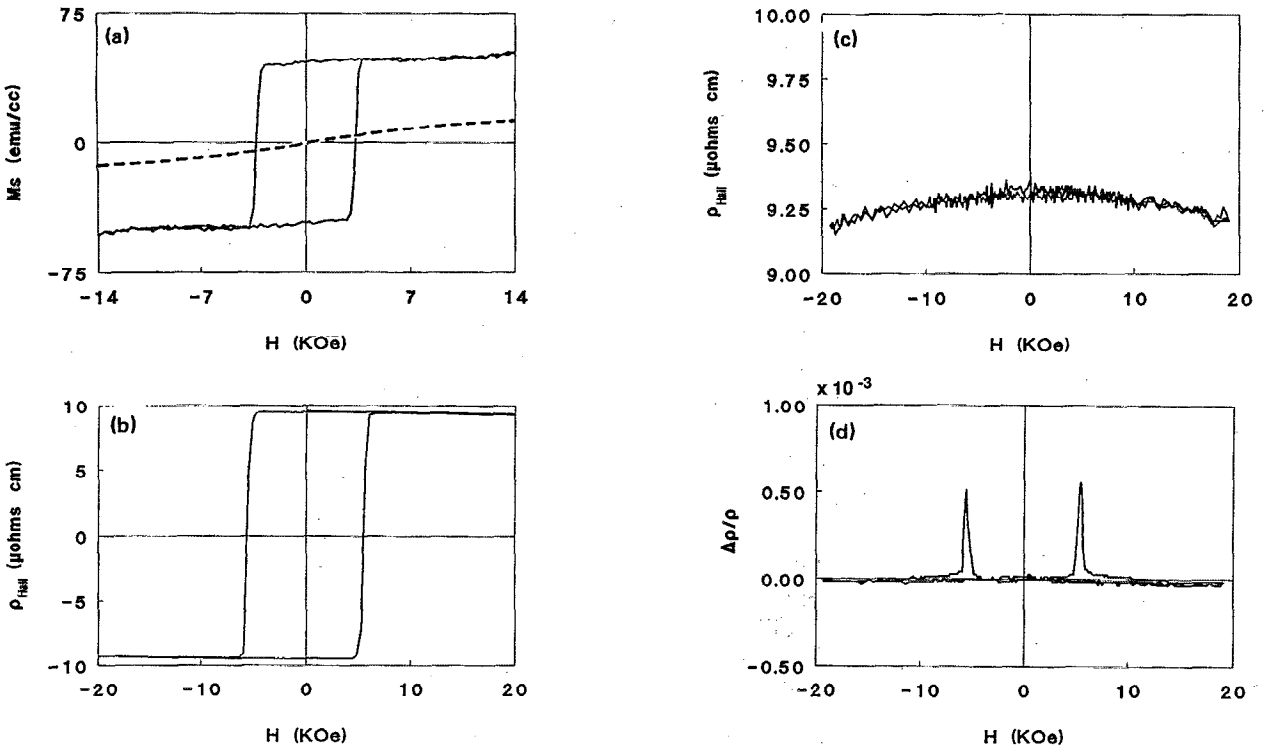

FIG. 7. Results of various measurements on a $Tb_{24}Fe_{76}$ sample with a thickness of 1040 Å. (a) VSM measurement with the magnetic field perpendicular (solid curve) and in the plane of the sample (dashed curve). (b) Hall resistivity vs the magnitude of an applied perpendicular field. (c) Hall resistivity vs the magnitude of an applied in-plane field. The sample is initially in the saturated state. (d) Resistivity variation as function of the magnitude of an applied perpendicular field.

E. Amorphous $Tb_{24}Fe_{76}$ film

The measurement results for this 1040-Å-thick sample, which is sputtered on a glass substrate, are shown in Fig. 7. The net magnetization of the film is $M_s = 54$ emu/cm^3 and its anisotropy field as extracted from the VSM data is $H_k \simeq 90$ kOe. When saturated along the easy axis, the sample exhibits a zero-field resistivity $\rho = 370$ $\mu\Omega$ cm, Hall resistivity $\rho_{xy} = 9.4$ $\mu\Omega$ cm, and Kerr rotation angle $\Theta_k = 0.27°$. The value of the anisotropy field derived from the in-plane Hall signal in Fig. 7(c) is $H_k \simeq 105$ kOe.

The MR curve in the perpendicular field has the usual peaks in the vicinity of H_c, but does not have a significant slope. This might indicate that the dispersion of Tb moments which, according to Kasuya's theory, could give rise to negative slopes for Tb-rich samples, is fairly small. Alternatively, the ordinary MR effects may be present, masking the effects of Tb moment dispersion.

F. Amorphous $Tb_{22.5}Fe_{77.5}$ film

The measurement results for this 930-Å-thick sample, which is sputter-deposited on a glass substrate, are shown in Fig. 8. Its saturation magnetization is $M_s \simeq 47$ emu/cm^3 and the sense of the Hall loop (or the magneto-optic Kerr loop) identifies the sample as Tb rich. The origin of the small jump in the VSM curves around $H = 0$ is not fully understood. However, since the Hall and the Kerr loops do not show a similar jump, we speculate that it might have arisen from the closure domains around the edges and corners of the sample. In the saturated state the zero-field resistivity is $\rho = 297$ $\mu\Omega$ cm, Hall resistivity is $\rho_{xy} = 5.7$ $\mu\Omega$ cm, and the Kerr angle is $\Theta_k = 0.27°$. The value of the anisotropy field derived from the in-plane Hall signal in Fig. 8(c) is $H_k \simeq 150$ kOe. The magneto-optic Kerr loop and the in-plane Kerr signal were identical to the Hall effect signals shown in Figs. 8(b) and 8(c) and are thus omitted.

In addition to the usual peaks around H_c, the perpendicular MR curve in Fig. 8(d) shows a small negative slope of 0.4×10^{-8} per Oe. One possible explanation for this negative slope is that it is caused by small pockets of high-coercivity material that slowly saturate as the field increases. The reduced dispersion of the terbium moment provides an alternative explanation. The longitudinal MR curve in Fig. 8(e) is small but, as expected, it increases with the increasing magnitude of the applied field. The transverse MR signal was too small to be measured for this sample.

G. Amorphous $Tb_{20.3}Fe_{76.8}Ar_{2.9}$ film

The measurement results for this 630-Å-thick sample, which is sputter-deposited on a glass substrate, are shown in Fig. 9. The sample's saturation moment is $M_s \simeq 50$ emu/cm^3 and the sense of the Hall loop (or the Kerr loop) identifies it as iron rich. The magneto-optic curves (omit-

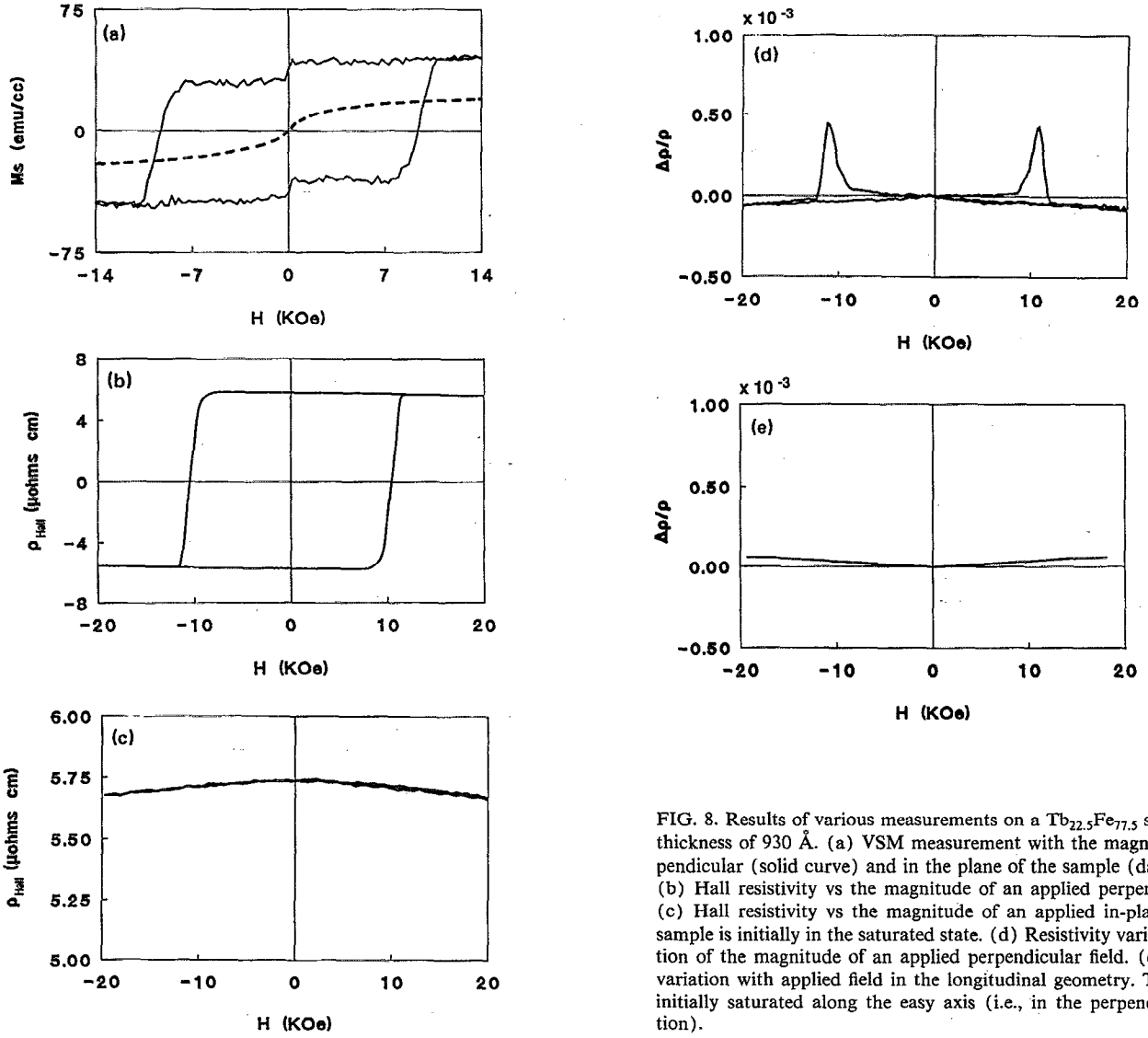

FIG. 8. Results of various measurements on a $Tb_{22.5}Fe_{77.5}$ sample with a thickness of 930 Å. (a) VSM measurement with the magnetic field perpendicular (solid curve) and in the plane of the sample (dashed curve). (b) Hall resistivity vs the magnitude of an applied perpendicular field. (c) Hall resistivity vs the magnitude of an applied in-plane field. The sample is initially in the saturated state. (d) Resistivity variation as function of the magnitude of an applied perpendicular field. (e) Resistivity variation with applied field in the longitudinal geometry. The sample is initially saturated along the easy axis (i.e., in the perpendicular direction).

ted) are identical to the Hall curves, but the differences between the VSM loop and the Hall loop are striking. Both the VSM loop and the Hall loop show the presence of an in-plane component of magnetization. When saturated along the easy axis, the sample has zero-field resistivity $\rho = 190\ \mu\Omega$ cm, Hall resistivity $\rho_{xy} = 2.6\ \mu\Omega$ cm, and Kerr angle $\Theta_k = 0.26°$. The anisotropy field derived from the reversible part of the in-plane Hall curve in Fig. 9(d) is $H_k \simeq 6$ kOe, corresponding to the relatively small value of $K_u \simeq 1.7 \times 10^5$ erg/cm^3.

In addition to the usual peaks around H_c, the perpendicular MR signal in Fig. 9(e) shows the effects due to the in-plane component of magnetization at small values of H, and a positive slope of about 0.7×10^{-8} per Oe at large H. The positive slope might be due to an increase in Tb moment dispersion which, in this iron-rich sample, is antiparallel to the field (Kasuya's model). The possibility of the ordinary MR effects making a contribution to this positive slope cannot be ruled out either. The longitudinal MR curve in Fig. 9(f) continues to rise well beyond the anisotropy field H_k. Again, this may be a consequence of the increasing Tb moment dispersion, but we do not fully understand it. In the transverse MR data of Fig. 9(g) the initial drop in $\Delta\rho/\rho$ is due to the alignment of the in-plane component of magnetization with the applied field. The subsequent rise in this signal is comparable with the rise in the perpendicular MR signal of Fig. 9(e), raising the possibility that the two signals are related and have the same physical origins.

H. Amorphous $Tb_{18.3}Fe_{74.5}Ar_{7.2}$ film

The measurement results for this 550-Å-thick sample, which is sputter-deposited on a glass substrate, are shown in Fig. 10. The sample is obviously iron-rich with perpendicular easy axis, saturation moment $M_s = 135$ emu/cm^3, and anisotropy field (extracted from VSM data) $H_k \simeq 19$ kOe. When saturated along the easy axis, the sample has zero-field resistivity $\rho = 275\ \mu\Omega$ cm, Hall resistivity $\rho_{xy} = 4.6\ \mu\Omega$ cm, and Kerr rotation angle $\Theta_k = 0.26°$. The plot of Hall resistivity versus the in-plane field in Fig. 10(c) is reversible up to $H \simeq 15$ kOe, and gives the estimate

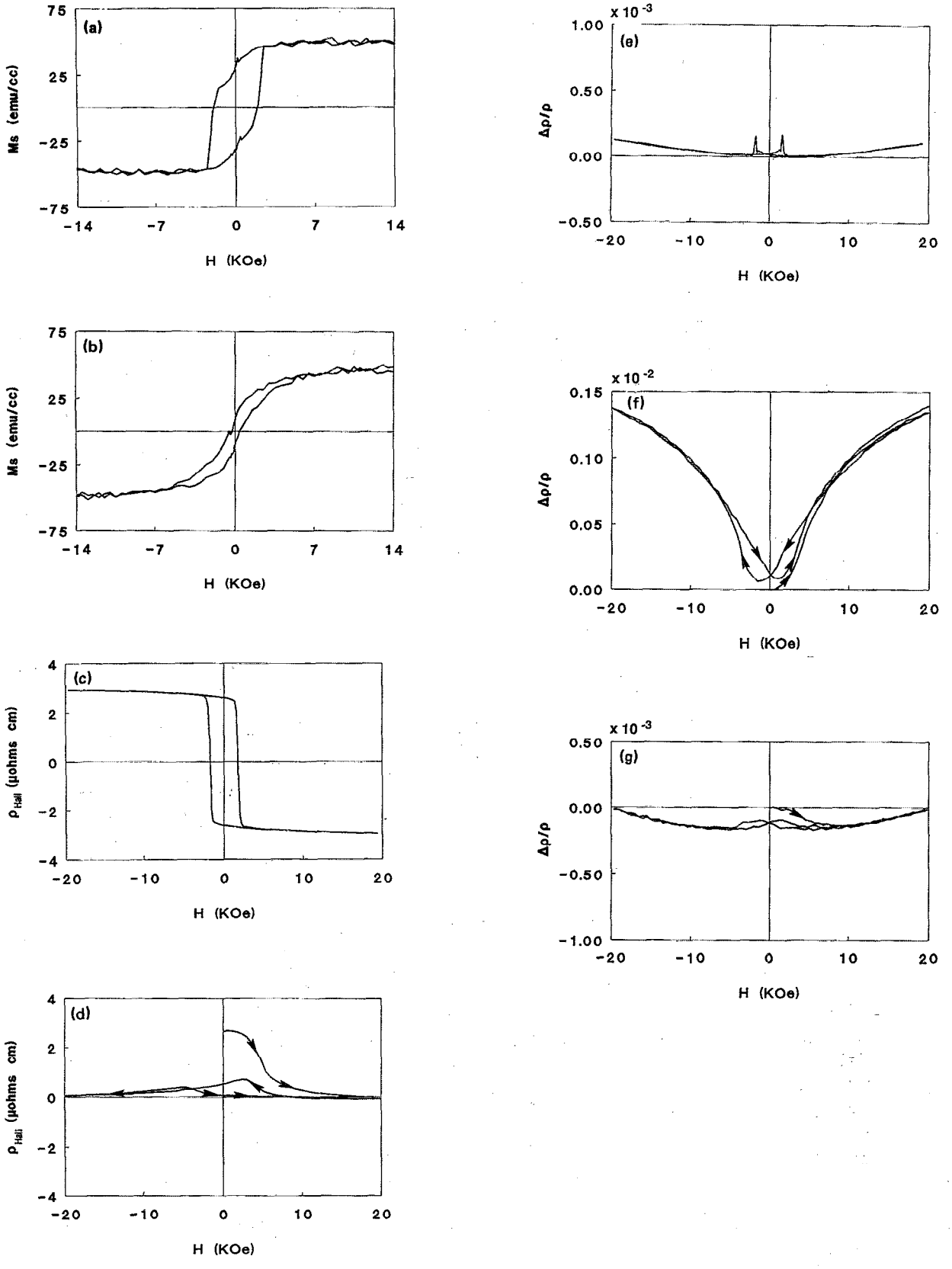

FIG. 9. Results of various measurements on a $Tb_{20.3}Fe_{76.8}Ar_{2.9}$ sample with a thickness of 630 Å. (a) VSM measurement with field perpendicular to the plane of the sample. (b) VSM measurement with in-plane field. (c) Hall resistivity vs the magnitude of an applied perpendicular field. (d) Hall resistivity vs the magnitude of an applied in-plane field. (e) Resistivity variation as function of the magnitude of an applied perpendicular field. (f) Resistivity variation with applied field in the longitudinal geometry. The sample is initially saturated along the easy axis (i.e., in the perpendicular direction). (g) Resistivity variation with applied field in the transverse geometry.

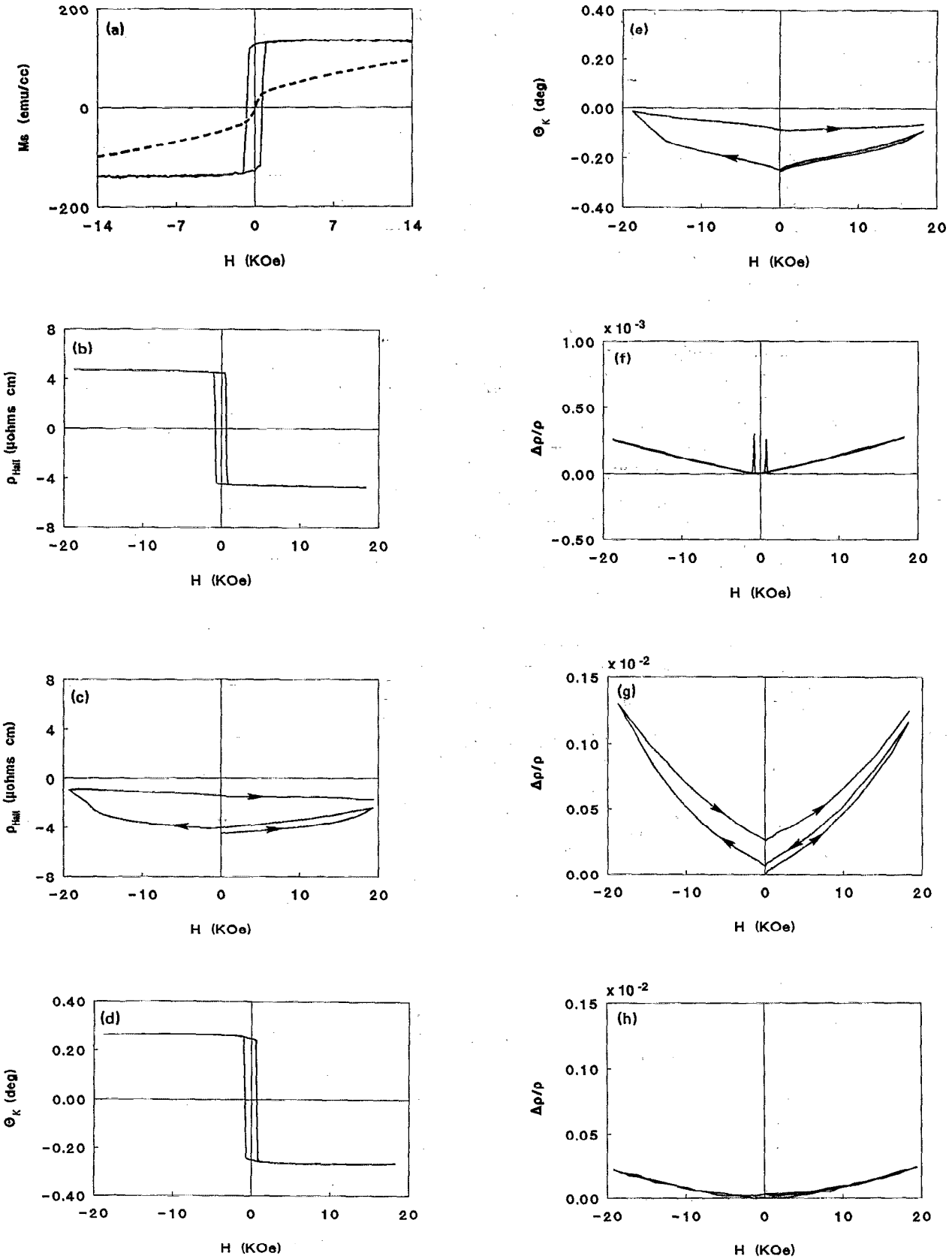

FIG. 10. Results of various measurements on a $Tb_{18.3}Fe_{74.5}Ar_{7.2}$ sample with a thickness of 550 Å. (a) VSM measurement with the magnetic field perpendicular (solid curve) and in the plane of the sample (dashed curve). (b) Hall resistivity vs the magnitude of an applied perpendicular field. (c) Hall resistivity vs the magnitude of an applied in-plane field. The sample is initially in the saturated state. (d) Magneto-optic polar Kerr signal vs the magnitude of an applied perpendicular field. (e) Magneto-optic polar Kerr signal vs the magnitude of an applied in-plane field. The initial state of the sample is saturated. (f) Resistivity variation as function of the magnitude of an applied perpendicular field. (g) Resistivity variation with applied field in the longitudinal geometry. The sample is initially saturated along the easy axis. (h) Resistivity variation with applied field in the transverse geometry.

of $H_k \simeq 21$ kOe for the anisotropy field. The in-plane Kerr signal is somewhat different from the corresponding Hall signal, as shown in Fig. 10(e).

In addition to the usual peaks around H_c, the perpendicular MR signal in Fig. 10(f) shows a positive slope of 1.6×10^{-8} per Oe. Since the sample is iron rich, this slope cannot be due to *s-d* scattering. (The scattering of the conduction *s* electrons into the *d* band of iron could, in principle, give rise to a positive slope for Tb-rich samples and a negative slope for Fe-rich samples. We, however, have not seen any of these manifestations of the *s-d* effect in our iron-based samples.) There are at least two plausible explanations for the positive slope, however. One possibility is that the dispersion of the Tb moment in this iron-rich sample increases with the increasing field. This explanation, which is based on Kasuya's model, would then require that the slope reverse its sign upon crossing H_c. Unfortunately, the resolution of the signal for $H < H_c$ is insufficient for the verification of this point. Another possibility is that the rise in $\Delta\rho/\rho$ in an increasing field is caused by the ordinary MR effects. Since the ordinary effects should be rather insensitive to the small changes in composition, the fact that our Tb-rich samples (which after all were only slightly richer in Tb) did not exhibit a positive slope is strong indication that the ordinary MR effects are not at work here.

Figure 10(g) shows the strength of the longitudinal MR signal versus the applied field. The relatively large magnitude of this signal is mainly due to the alignment of the magnetic moments with the direction of the current. Finally, in Fig. 10(h) we show the transverse MR signal versus the applied field. The magnitude of this signal is comparable with the perpendicular MR signal in Fig. 10(f), which leads us to believe that the two are rooted in the same physical processes. Again, more work is needed in order to sort out the various phenomena and understand them in detail.

V. CONCLUDING REMARKS

We have reported the results of magnetoresistance measurements on a number of thin-film samples of Co/Pt, Co/Pd, and Tb_xFe_{1-x}. Supplementary data from vibrating sample magnetometry, magneto-optic Kerr-effect measurements, and the measurement of the Hall effect were also presented. Various contributions to magnetoresistance were identified and their relationship to the magnetic structure/micromagnetic properties of the media were discussed. Among the intriguing possibilities suggested by the data so far, we mention a significant contribution by paladium to the *s-d* scattering in Co/Pd superlattice films, and the manifestation of terbium moment dispersion in Fe-rich amorphous films of TbFe.

ACKNOWLEDGMENTS

The authors are grateful to Dr. C. J. Lin of IMB's Almaden Research Center and to Dr. C. Brucker of Kodak Research Laboratories for providing the superlattice samples. Thanks are also due to Professor C. Falco, Dr. B. Engel, M. C. England, and M. R. VanLeeuwen for many helpful discussions. This work has been supported by a grant from the IBM Corporation and, in part, by the Optical Data Storage Center at the University of Arizona. One of us (R. A. H.) would also like to acknowledge the support of an IBM fellowship.

[1] W. Thomson, Proc. R. Soc. London **8**, 546 (1857).
[2] N. F. Mott, Proc. R. Soc. London Ser. A **153**, 699 (1936), and **156**, 368 (1936).
[3] T. Kasuya, Prog. Theoret. Phys. (Kyoto) **16**, 58 (1956).
[4] J. P. Jan, *Solid State Physics* edited by F. Seitz and D. Turnbull (Academic, New York, 1957), Vol. 5.
[5] S. V. Vonsovskii, *Magnetism* (Keter, Jerusalem, 1974).
[6] J. Smit, Physica **17**, 612 (1951).
[7] J. Kondo, Prog. Theoret. Phys. (Kyoto) **27**, 772 (1962).
[8] T. R. McGuire and R. I. Potter, IEEE Trans. Mag. **MAG- 11**, 1018 (1975).
[9] S. Yumoto, K. Toki, O. Okada, and H. Gokan, IEEE Trans. Magn. **MAG-24**, 2793 (1988).
[10] A. B. Pippard, *Magnetoresistance in Metals* (Cambridge University Press, Cambridge, 1989).
[11] D. A. Thompson, L. T. Romankiw, and A. F. Mayadas, IEEE Trans. Magn. **MAG-11**, 1039 (1975).
[12] P. Wolniansky, S. Chase, R. Rosenvold, M. Ruane, and M. Mansuripur, J. Appl. Phys. **60**, 346 (1986).
[13] E. C. Stoner and E. P. Wohlfarth, Philos. Trans. R. Soc. London Ser. A **240**, 599 (1948).
[14] L. J. van der Pauw, Philips Tech. Rev. **20**, 220 (1958).